ASPIRE Parachute Modeling and Comparison to Post-Flight Reconstruction

Soumyo Dutta*
NASA Langley Research Center, Hampton, VA 23681, USA

The Advanced Supersonic Parachute Inflation Research and Experiment (ASPIRE) was a series of sounding rocket flights aimed at understanding the dynamics of supersonic parachutes that are used for Mars robotic applications. Three flights for ASPIRE occurred off the coast of Wallops Island, VA in Oct. 2017, Mar. 2018, and Sept. 2018 and successfully demonstrated deployment and inflation of the Mars Science Laboratory and Mars 2020 mission parachute. Prior to all three flights, a multi-body flight dynamics simulation was developed to predict the parachute dynamics and was used, in conjunction with other tools, to target Mars-relevant flight conditions. After each flight, the reconstructed trajectory was used to validate the pre-flight dynamics simulation and recommend changes to improve predictions for future flights in the ASPIRE program. This paper describes the parachute models and flight mechanics simulation used to target conditions for the three flights and the post-flight comparison of the tools.

I. Introduction

In 2017 and 2018, NASA tested three supersonic parachutes off the coast of Virginia near NASA Wallops Flight Facility (WFF) to help quantify the performance of the parachute that will be used during entry, descent, and landing for the Mars 2020 mission on Feb. 2021. The tests were part of a series of sounding rockets flights for the Advanced Supersonic Parachute Inflation Research and Experiment (ASPIRE) program that was started in 2016 to understand the inflation and peak load performance of supersonic parachutes used for Mars robotic missions.

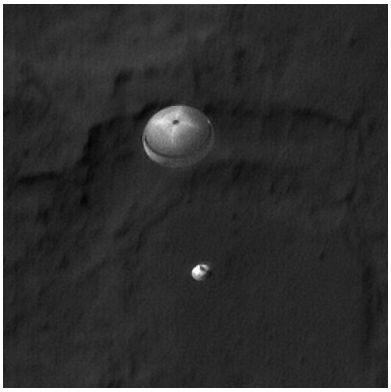

Fig. 1 The MSL DGB parachute. (Image Credit: NASA/JPL-Caltech/Univ. of Arizona)

The 2012 Mars Science Laboratory (MSL) mission had a successful inflation of its supersonic disk-gap-band (DGB) shaped parachute, shown in Fig. 1. In 2014 and 2015, the Low Density Supersonic Decelerator (LDSD) program conducted two flight tests with Ringsail parachutes at an inflation Mach number greater than 2.0, but the tests suffered failure in the parachute during the inflation process. The LDSD tests raised questions about the understanding of parachute inflation and dynamics at Mars relevant conditions. The Mars 2020 project established the ASPIRE tests as a risk mitigation program to qualify its supersonic parachute.

The main objective of the ASPIRE program was to certify a 21.5 m DGB parachute for use at Mars. The ASPIRE project tested two designs: the built-to-print MSL design and a strengthened parachute design that increased margins in the strength of the parachute canopy cloth [1]. The project had three test flights, with the built-to-print MSL design tested on the first flight and the new strengthened design tested on the last two flights. The success of the new parachute design led to Mars 2020 adopting the strengthened parachute for flight.

This paper will provide an introduction to the ASPIRE flight project, its concept of operations, and discuss the flight mechanics and parachute models. Finally, the simulation results will be compared with the post flight reconstructed performance of the three ASPIRE flights.

*Aerospace Engineer, Atmospheric Flight and Entry Systems Branch, 1 N. Dryden St., M/S 489, and AIAA Senior Member.

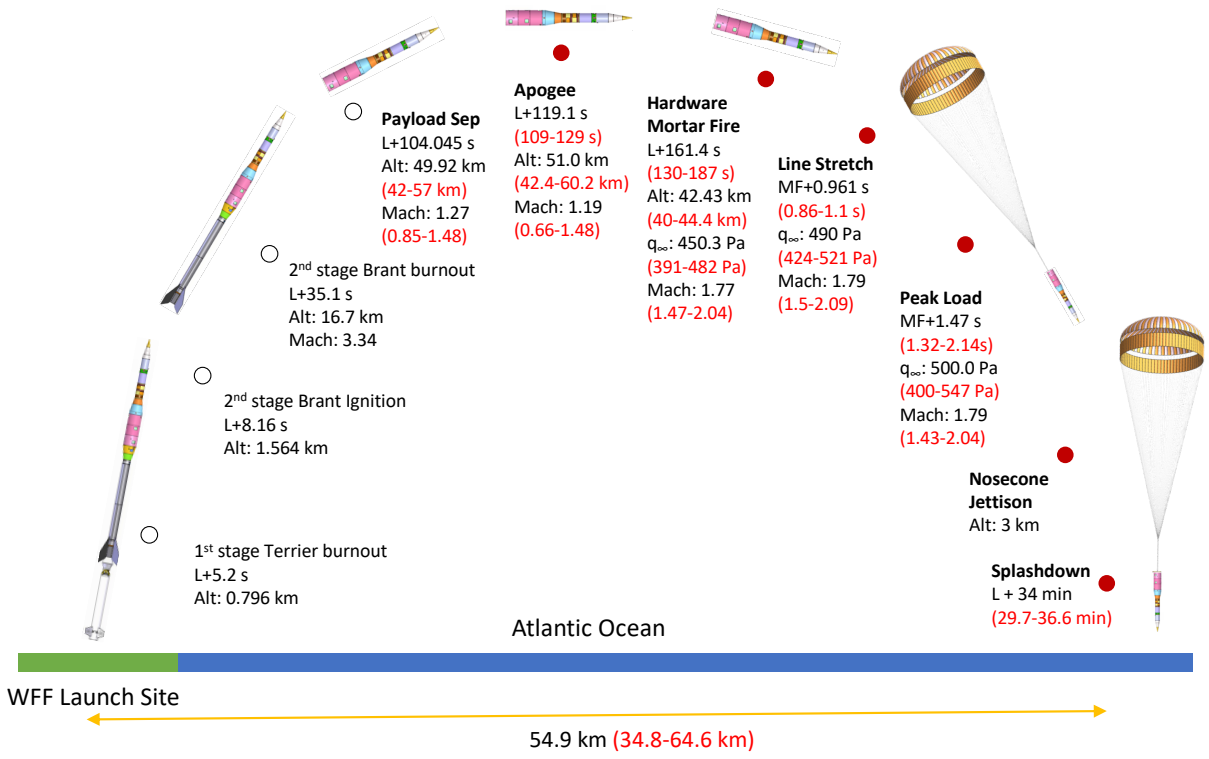

Fig. 2 ASPIRE concept of operations. The reconstructed values in black and pre-flight min/max predictions in red are for SR01 flight.

II. ASPIRE Flight Project

The ASPIRE flight concept of operations is shown in Fig 2. The test vehicle and parachute are launched on-board sounding rockets under NASA's Sounding Rocket Operations Contract (NSROC). For ASPIRE, the sounding rocket stack (as shown in Fig. 3) consists of a Terrier first stage, a Black Brant IX second stage, and a payload comprised of a 1200 kg test vehicle that includes the parachute system. At payload separation, which occurs 104 s from launch, the vehicle is approximately Mach 1.2 and at 50 km altitude. After payload separation, the test vehicle reaches apogee at approximately 51 km.

The first ASPIRE flight - SR01 - targeted conditions similar to the MSL as-flown values. The dynamic pressure targeted at full inflation was 474 Pa and the Mach number targeted was 1.7 [2]. For SR02, the target was approximately 50% larger dynamic pressure than MSL flight conditions; thus, the target full inflation dynamic pressure was 678 Pa while the target Mach number at full inflation was still close to Mach 1.7. For SR03, the target was two times the parachute load experienced by the MSL parachute in 2012; thus, the target parachute load was 70,000 lbf, which was equivalent to approximately 1000 Pa at full inflation.

After the parachute inflates, the vehicle decelerates rapidly to subsonic conditions and finally splashes down in the Atlantic Ocean approximately 60 km East from WFF. Shortly before splashdown, the vehicle ejects the heavily weighted nosecone to improve the buoyancy of the rest of the payload. The nosecone has ballast to improve the conditions that can be achieved at parachute deployment.

The test vehicle is shown in Fig. 3. The payload is 6.66 m in length and 0.72 m diameter at its largest cross-section. The front portion of the vehicle consists of the ballast and buoyancy foam, while the back end consists of the mortar and other parachute deployment systems. The vehicle contains an attitude control system called NSROC Inertial Attitude Control System (NIACS), which uses information from the inertial measurement unit (IMU) called the Gimbaled LN-200 Miniature Flight Computer (GLN-MAC). Both of these systems are housed aft of the buoyancy foam and ahead of the parachute system. In early flight mechanics analysis, it was discovered that active attitude control is needed to maintain the vehicle at the desired attitude at the start parachute deployment. However, in order to observe the inflation of the parachute unhampered by an attitude control system, the NIACS is turned off at mortar fire to allow the dynamics

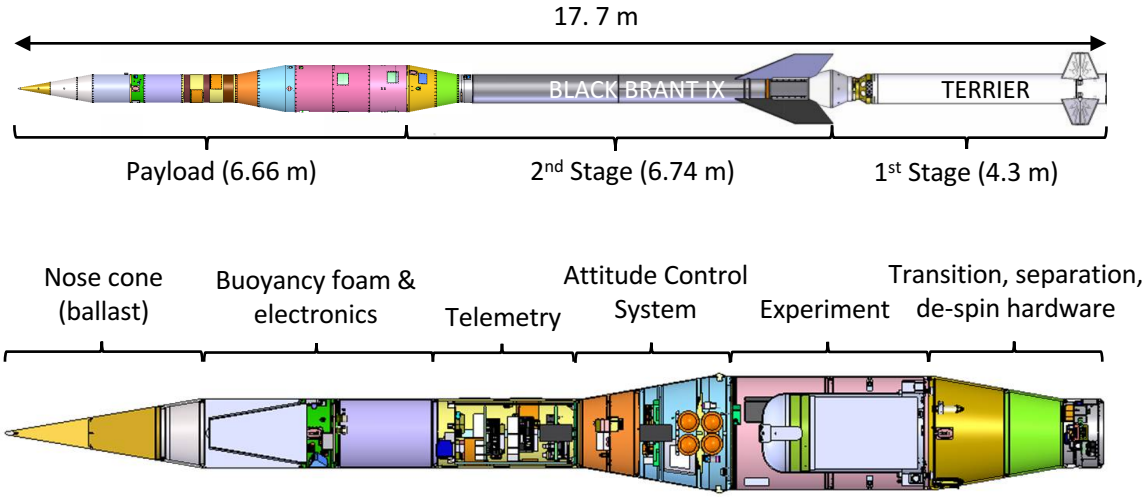

Fig. 3 ASPIRE flight vehicle configuration.

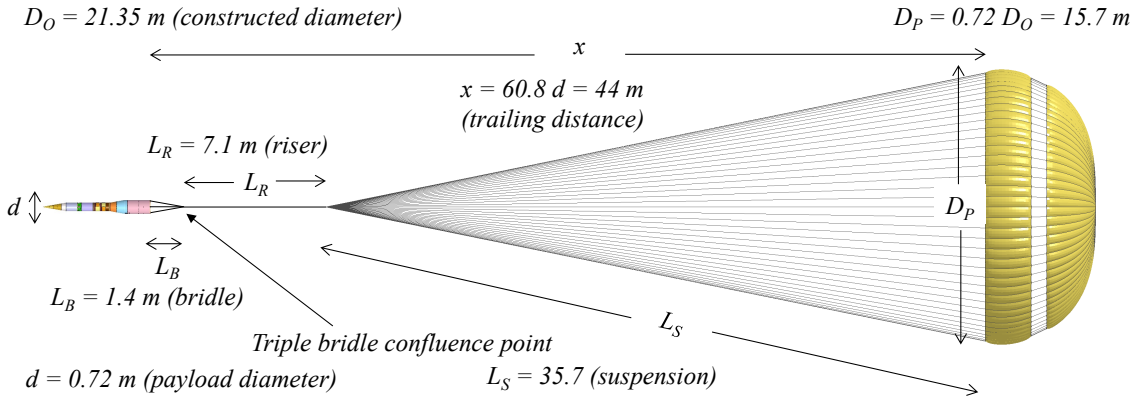

Fig. 4 ASPIRE test vehicle and SR01 parachute system. The dimensions of the SR02 parachute were similar although the fabric strengths were higher.

of the parachute and its effect on the test vehicle to be observed without any external moments.

The test article for ASPIRE SR01 was the MSL-heritage DGB parachute. The dimensions of the various components of the final test configuration are shown in Fig. 4. The final constructed diameter of the parachute for ASPIRE SR01 was 21.35 m and the projected diameter was 15.7 m. For SR02 and SR03, the test article was a strengthened DGB parachute designed for the Mars 2020 mission [1]. The dimensions of the parachute were similar to the SR01 article, although the mass of the parachute was higher due to the use of strengthened fabrics and the mortar force was higher to compensate for the heavier parachute.

Reference [1] discusses the difference between the two types of parachutes used in ASPIRE. For all flights, the test vehicle was attached to the parachute canopy via bride, riser, and suspension lines, as shown in Fig. 4. The three lines directly attached to the back end of the test vehicle are the bridle lines, which come together at a triple bridle confluence point (TBCP). The riser lines connect the TBCP to the suspension lines. These lines provide a variety of stiffness and damping between the parachute canopy and the rigid test vehicle.

In the next section, the parachute force model is discussed and in Sec. IV, the multi-body system model is described.

III. Parachute Aerodynamics Modeling

A. Drag Modeling

O'Farrell et al. [3] conducted a survey of past wind tunnel tests, flight tests, and Mars missions that used DGBs with a Viking-like geometry: a geometric porosity (λ_G) of 12.5% and a ratio of suspension line length to nominal diameter (L_{SL}/D_0) of 1.7. Relevant results from that study are reproduced in Figs. 5- 8.

Table 1 Summary of prior wind tunnel tests of Viking-like DGBs.

Facility	D_0 (m)	Mach	λ_g (%)	D_0/d	x/d	L_{SL}/D_0	Reference
AEDC 16S	1.62*	1.8 - 2.6	12.5	4.61	8.5	1.7	
AEDC 16T	1.62§	0.2 - 1.4	12.5	4.69	8.5	1.7	AEDC TR-72-78 [4]
	1.62†	0.2 - 1.4	12.5	29.4	8.53	1.73	
LaRC TDT††	1.43‡	0.1 - 0.5	12.0	4.82	10.3	1.7	NESC 14-00932 [5]
GRC 10'×10'	0.81§§	2.0 - 2.5	12.5	4.76	10.6	1.7	AIAA 2008-6217 [6]

∗ Parachute tested in the wake of Viking entry vehicle (VEV) forebody.
§ Parachute tested in the wake of Viking lander (VL) forebody.
† Parachute tested without a forebody model (NF).
‡ Parachute tested in the wake of MSL backshell forebody.
†† Tested models constructed from fabrics of two permeabilities: PIA-C-7020 and PIA-C-44378.
§§ Parachute tested in the wake of MSL entry vehicle forebody.

Figure 5 shows the reconstructed drag coefficient (C_D) from all wind tunnel tests of Viking-like DGBs. Table 1 provides details of these tests, including the model size and geometric porosity, test conditions, suspension line length, forebody diameter (d), and parachute trailing distance (x). Note that five of the datasets correspond to parachutes tested in the wake of a blunt forebody model, while a single dataset corresponds to a parachute tested in the wake of a slender test fixture only. Note also that [5] tested model parachutes from two different fabrics: a fabric with MSL-like permeability (PIA-C-7020D Type I) and a fabric with almost zero permeability (PIA-C-44378D Type I) that exhibited significantly higher drag. The Mars 2020 and MSL parachutes have different permeability and testing these two fabrics allowed the test to bracket the conditions expected on Mars for those two parachutes.

In Fig. 5, the parachute drag model from the MSL project is shown for reference. [3] found that the C_D of the Viking-like DGB tested in the wake of a slender sting only was between 1% and 12% higher than for similar parachutes tested in the wake of a blunt body. In addition, [7] conducted computational fluid dynamics (CFD) simulations of rigid canopies in the wakes of slender and blunt forebodies. [7] found the drag on parachutes in slender body wakes to be between 3% and 15% higher than on parachutes deployed behind blunt bodies. In addition, both [3] and [7] found evidence that the transonic parachute drag deficit was significantly reduced in slender body wakes.

As a result, the ASPIRE project developed a model for the C_D of Viking-like DGBs tested behind slender sounding rocket payloads. This model was based on the MSL drag model shown in Figure 5, but included the following changes:

- The nominal C_D curve was increased by 2.5% in the subsonic regime and 8% in the supersonic regime. The 8% increase was in the middle of the observed 3% and 15% higher C_D observed for parachutes deployed behind blunt bodies [7].
- The model bounds were widened to account for the scarcity of data for DGBs tested behind slender bodies.
- The decrease in C_D near Mach 1 was significantly reduced.

Figure 6 shows the ASPIRE C_D model along with data for all flight tests of Viking-like DGBs. The model is compared against the reconstructed C_D from DGBs deployed behind blunt bodies in Fig. 6(a), while Fig. -6(b) shows the reconstructed C_D from all three ASPIRE flight tests of DGBs behind slender bodies. The ASPIRE results are based on moving window average with bins of Mach 0.03. At subsonic speeds, the measured C_D during for the three ASPIRE flights was in good agreement with the ASPIRE model. At Mach numbers above 1.1, however, the reconstructed C_D was generally lower than the nominal pre-flight estimate. The reason for this discrepancy is currently being investigated and potential contributing factors have been identified. For example, the ASPIRE model relied on assumptions about the dynamics of the parachute payload system as well as CFD simulations of an inflated canopy in the wake of the payload

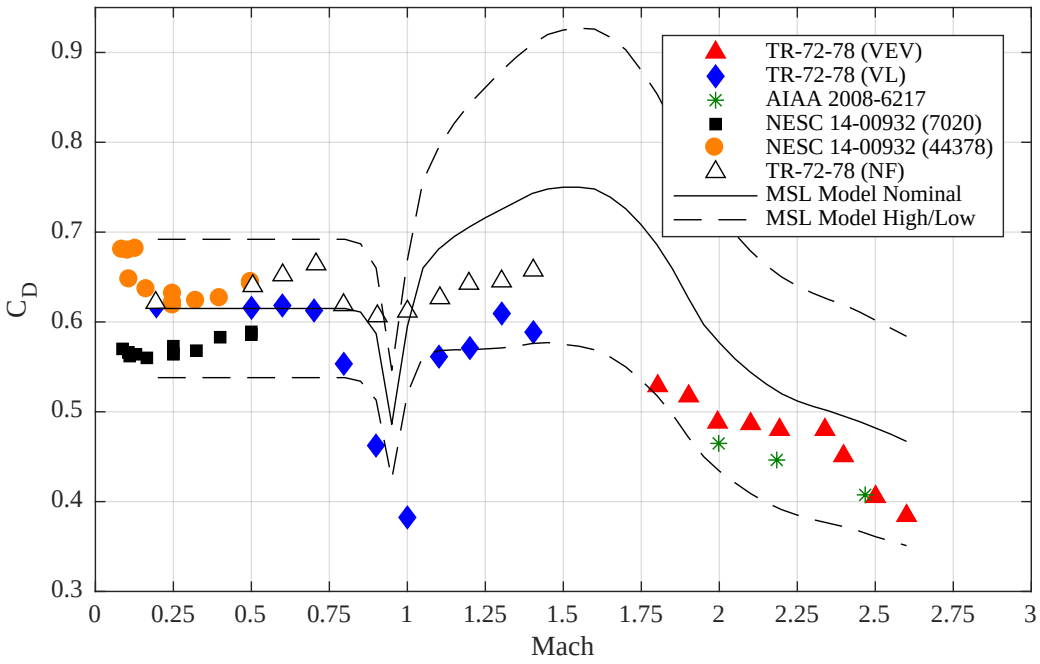

Fig. 5 Comparison of wind tunnel drag coefficient results for DGBs with Viking-like geometries, in the wake of blunt and slender bodies. The filled symbols represent the data from tests of parachute models in the wake of a blunt body, and the unfilled symbols represent the data for models tested in the wake of slender bodies.

which are sensitive to the choice of inflated geometry and location of the canopy within the wake. The stereoscopic reconstruction of the canopy shape will aid in improving these models.

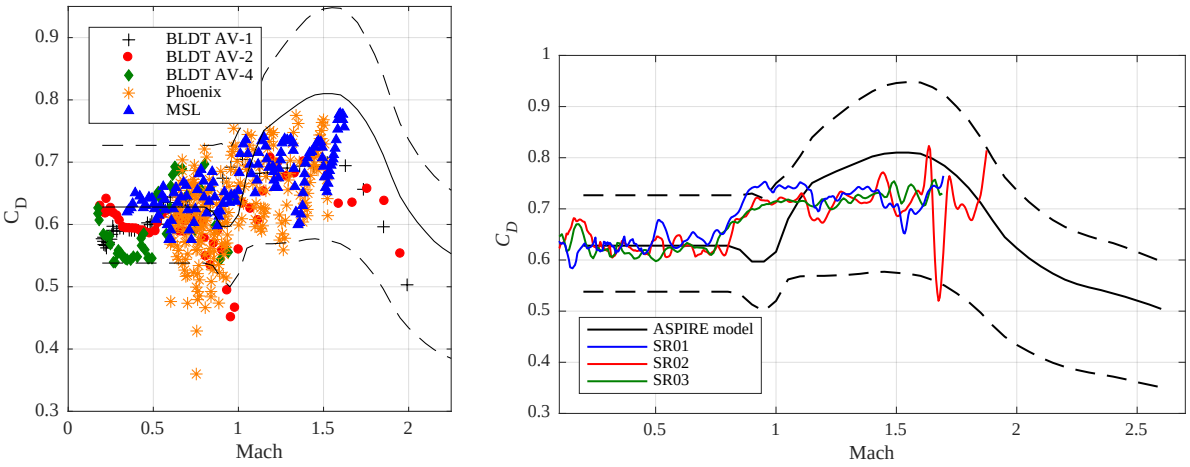

Fig. 6 C_D as a function of Mach number for flight tests of Viking-like DGBs in the wake of (a) blunt bodies, and (b) slender bodies. The solid black line denotes the nominal values for the ASPIRE drag model, while the black dashed lines represent the upper and lower model bounds.

B. Static Aerodynamics Modeling

Historically, most wind tunnel tests of parachute systems have focused only on the drag coefficient of the parachute. In 2014, the NASA Engineering and Safety Center (NESC) conducted a test of various scaled parachute models to address this deficiency [5, 8]. This test, which was very similar to a previous test conducted by the Mars Exploration Rovers (MER) project in 2001 [9], included testing of DGB models both in the wake of the MSL backshell and without the backshell forebody model. As discussed in Section III.A, [5] tested models constructed out of two fabrics with very different permeabilities. For the setup with the backshell forebody, tests were conducted at a variety of Mach and Reynolds numbers representative of terminal descent at Mars. However, for the setup without a backshell model, the parachutes were tested at a single test condition.

Figure 7 shows the parachute tangential (C_T) and normal (C_N) force coefficients, and the pitching moment coefficient about the confluence point of the parachute suspension lines (C_{m0}) for the model parachutes tested both with and without the forebody model. The black lines show the results for the models constructed using PIA-C-7020 Type I fabric, while the blue lines show the results for the near-zero permeability PIA-C-44378D Type I fabric. [10] combined these results with models for the permeability of the two fabrics [11] to develop a model for the static aerodynamic coefficients of DGBs in blunt body wakes as a function of Mach number and Reynolds number (within a range of conditions representative of terminal descent at Mars).

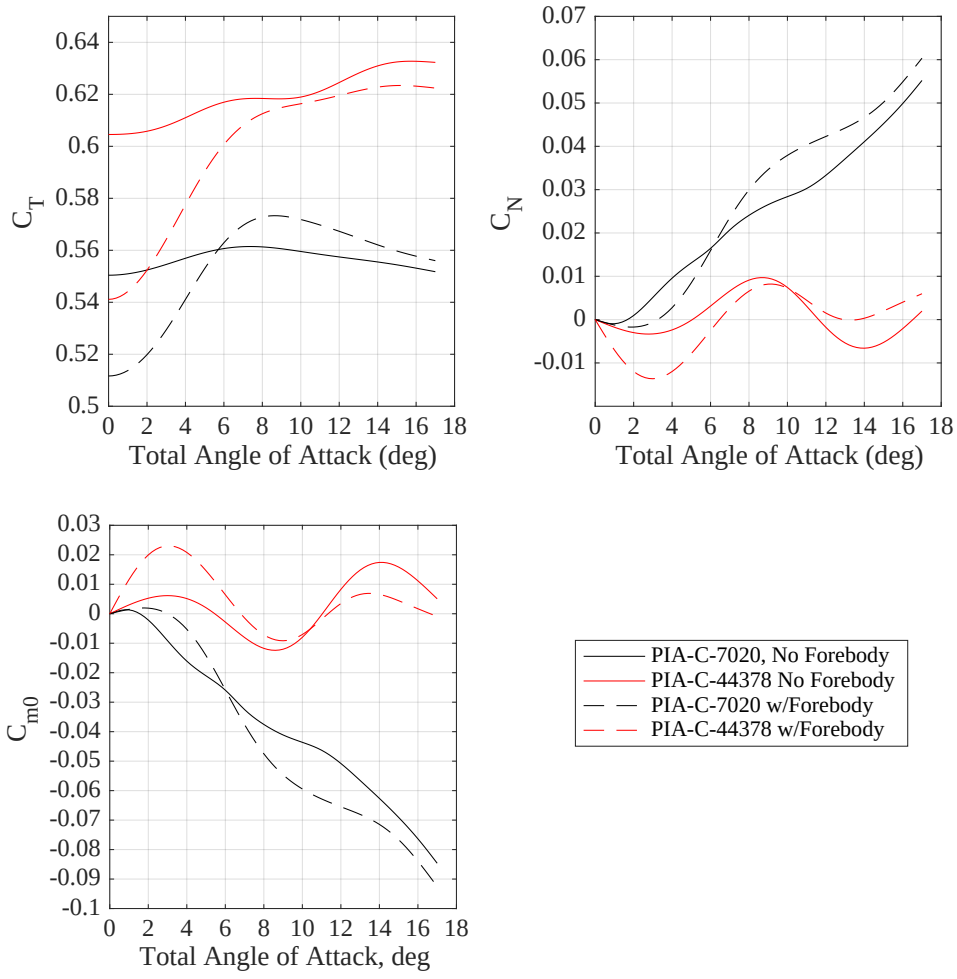

Fig. 7 Wind tunnel measurements of the static aerodynamic and moment coefficients for scale models of the MSL DGB constructed from two different fabrics: PIA-C-7020D Type I (black lines) and PIA-C-44378D Type I (red lines). The models were tested in the wake of a blunt forebody model (dashed lines) and in the wake of a slender test sting (solid lines).

The ASPIRE project sought to develop a similar model for the static aerodynamic coefficients tested behind slender bodies. However, the method of [10] could not be applied directly to the DGBs tested behind the slender sting in the NESC test, as data were only available at a single test condition. As a result, for the ASPIRE model the difference in the aerodynamic coefficients due to wake effects was independent of test condition but dependent on total angle of attack and fabric. From the results shown in Fig. 7, a wake-effect correction was calculated for each fabric type. After applying this correction, the method of [10] was used to develop the static aerodynamic model for DGBs in the wake of slender bodies shown in Fig. 8.

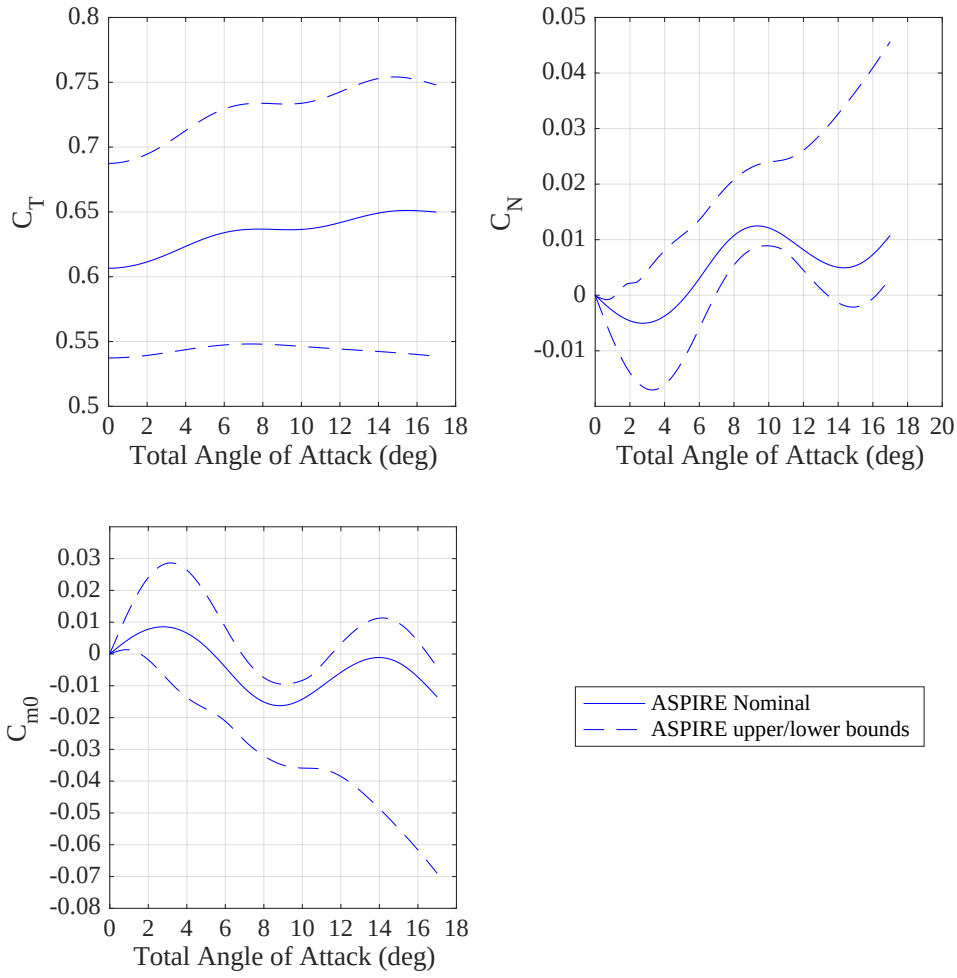

Fig. 8 ASPIRE model for the static aerodynamic coefficients of DGBs tested in the wake of a slender body.

IV. Flight Dynamics Modeling and Simulation

Pre-flight prediction of the vehicle performance and targeting of the mortar fire trigger to hit desired parachute performance were achieved via flight mechanics simulations that modeled various aspects of the flight profile from launch to splashdown. One of the tools used for parachute modeling is POST2, which is a six degree of freedom (6DOF) flight dynamics simulation tool that can simultaneously simulate the trajectory of up to 20 independent or connected rigid bodies. It is a generalized point mass, discrete-parameter targeting and optimization trajectory simulation program with multi-vehicle capabilities that integrates translational and rotational equations of motion along the trajectory. The simulation tool has significant entry, descent, and landing (EDL) flight heritage as it has been used in the past successfully for several Mars EDL missions, such as Mars Pathfinder [12], Mars Exploration Rovers [13], Mars Phoenix [14], and Mars Science Laboratory [15]. Additionally, POST2 simulations were also used on the LDSD flights 1 [16–18] and

2 [19, 20].

The ASPIRE simulation is based on the POST2 simulation used in LDSD to model the multi-body dynamics of the flight article. The simulation incorporates various engineering models for the vehicle and the environment. These models include vehicle mass properties, mortar fire orientations, CFD-based aerodynamic predictions of the test vehicle during flight, parachute aerodynamics based on wind tunnel tests, flight software used for triggering mortar fire during flight, the NIACS, and atmospheric property predictions initially from Earth Global Reference Atmospheric Model (Earth-GRAM 2010) [21] and later from NASA Goddard Earth Observing System model version 5 (GEOS-5) [22]. The models and their uncertainties are varied in Monte Carlo analysis to provide statistical estimates of various flight performance parameters, such as trajectory conditions at parachute full inflation and splashdown predictions.

The POST2 multi-body dynamics model is based on simulating the response between two rigid, 6DOF vehicles connected by lines. For ASPIRE, the two 6DOF rigid bodies are the test vehicle and the parachute, which are connected by tension-only bridle lines that have stiffness and damping. Treating the parachute as a rigid vehicle is a key assumption as it is modeled as a single vehicle from the TBCP up to the canopy with mass properties that include the mass of the canopy, suspension lines, and riser lines. In reality, the parachute is a flexible body while the suspension lines and riser line also have their own mass, stiffness, and damping. However, multi-body simulations used for other flight projects in the past have shown that modeling the parachute down to the TBCP as a rigid body and then connecting that body to the forebody via tension-only bridle lines provides an attitude and force response that is comparable to flight data. [2] Thus, for ASPIRE, the same assumptions were made.

The multi-body phase of the modeling starts at mortar fire, when a test vehicle ejects the parachute bag using the mortar engine. The mortar is modeled as a thruster that applies a constant force on both the parachute bag and the test vehicle for a finite time. The mortar thrust direction can be varied based on alignment uncertainty for Monte Carlo analysis. The parachute bag, which is a 3DOF vehicle, is pushed along the length of the parachute can until it fully exits from the separation plane of the test vehicle. While the bag is in the parachute can, a constraint force equations (CFE) based model [23] is used to constrain the motion of the bag axially and also simulate the friction on the bag. The initial phase of the multi-body dynamics is shown in Fig. 10(a).

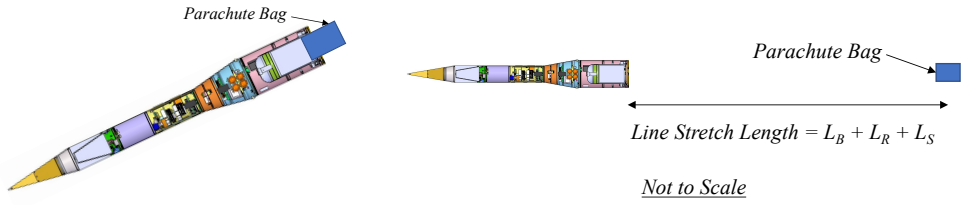

(a) Mortar Fire (b) Line Stretch

Fig. 9 Multi-body model dynamics for ASPIRE.

After the parachute bag exits the test vehicle, the only force acting on this vehicle are gravity. In reality the bag experiences aerodynamic drag; however, this force is very difficult to model with CFD tools given the bag is in the unsteady wake of the test vehicle. Assuming no drag provides a conservative estimate of the time to the line stretch event.

Upon reaching the line stretch distance, shown in Fig. 9(b), the parachute bag vehicle is replaced by the 6DOF rigid parachute body. The line stretch distance is the sum of bridle lines length (L_B), riser line length (L_R), and suspension lines length (L_S). Recall, the parachute vehicle starts at the TBCP, where the three bridle lines provide the connection to the test vehicle via tension-only lines. The stiffness and damping of the tension lines are based on properties of the actual bridle lines.

The parachute bag is treated as a 3DOF vehicle whose attitude is not tracked; therefore, when the parachute vehicle is initialized at line stretch, its attitude is prescribed as an angle relative to the payload that is varied in a Monte Carlo simulation. This angle, called the apparate angle, is typically informed by previous flight data and wind tunnel tests. However, most DGB test data consist of a blunt body forebody similar to entry aeroshells. Blunt bodies have larger wakes than the relatively slender body of the ASPIRE test vehicle. Thus, the parachute initialization angle choice for ASPIRE was a mixture of previous data and engineering judgment.

Once the line stretch condition has been achieved and the parachute vehicle has been initialized, the two rigid bodies behave under their separate aerodynamics while responding to each other due to forces from the lines connecting

them. The test vehicle aerodynamics is discussed by Muppidi et. al. [24]. The parachute aerodynamics is discussed in Sec. III.A.

During inflation, the parachute aerodynamic force changes from zero at line stretch to peak load at full inflation based on a power law dependent on time since line stretch and time to full inflation. [25] The inflation time itself is based on the distance it takes for the parachute to travel a fixed inflation distance [26] which is determined empirically and varied in Monte Carlo analysis.

After the full inflation time has elapsed, the configuration in the simulation looks similar to what is shown in Fig. 4. At full inflation, other models are turned on in the simulation. The parachute has inflated by capturing a volume of atmosphere. This captured atmosphere adds to the parachute mass as so-called apparent mass. The captured atmosphere also provides a buoyant force to the vehicle. These forces are activated at full inflation since their effects are captured during the inflation process by the opening load factor that is applied to the aerodynamic force. Additionally, while the parachute vehicle is above Mach 1.4 it experiences areal oscillation, where the force of the vehicle fluctuates based on a random process that simulates the collapse and re-inflation of the canopy observed during the deployment of supersonic parachutes in the past. Cruz et. al. discuss the parachute model in great detail in Ref. [25], while Way describes the inflation dynamics in [27].

V. Pre-Flight Predictions and Comparison with Flight Data

The three ASPIRE flight vehicles had many different instruments on-board to assist in post flight reconstruction of the trajectory. [28] The IMU on GLN-MAC recorded the acceleration and angular rates sensed on-board the test vehicle at a rate of 400 Hz. The test vehicle was also equipped with a global positioning system (GPS) receiver that provided updated position and velocity states. The vehicle was tracked using an on-board C-Band transponder and by skin tracking from three WFF radars. The ASPIRE vehicle also had a pair of situational GoPro cameras and another pair of high resolution, high-speed cameras that provided good videos of the inflation process. Moreover, multiple high altitude balloons with radiosondes captured atmospheric profile data up to 40 km altitude on the day of launch.

The IMU, GPS, radar, and balloon data were used within an Extended Kalman Filter based tool, called New Statistical Estimation Program (NewSTEP), to provide a post flight best estimated trajectory [29, 30]. In the following sections, ASPIRE SR01, SR02, and SR03 reconstructed trajectories are compared with pre-flight Monte Carlo estimates. In most instances, the reconstructed flight conditions fell well within the pre-flight Monte Carlo distributions that provided statistical estimates of conditions at major events of interest. However, in cases where the pre-flight estimates fail to match the reconstruction, the process of reconciliation was undertaken to adjust the pre-flight models in order to understand what components of the simulation should be modified to better capture the mechanics of reality. Reconciliation of the ASPIRE flights is discussed in [31], where it was found that updating the simulation initial conditions to actual separation states and atmospheric models to as-observed atmosphere reconciled most differences between pre-flight predictions and as-flown conditions.

The following sections focus on specific components of parachute modeling and leverage the reconstruction and reconciliation work discussed in the aforementioned references.

A. Parachute Loads

The key goal for ASPIRE was to qualify the Mars 2020 parachute to flight relevant conditions. A primary metric was for the flights to target a specific parachute load and the parachute to successfully inflate at these conditions. The SR01 flight recreated the MSL as-flown conditions, while the SR02 and SR03 parachutes were targeted to 100% and 140% of the expected flight limit load for Mars 2020. Table 2 lists the dynamic pressure and parachute loads targeted by the three flights.

MSL flight history and reconstruction showed that the predicted parachute load at full inflation was overestimated by the load indicator used for that mission. [25] That load indicator was based on an opening load factor (C_x) of 1.4 and was a function of the flight environment conditions, such as dynamic pressure and Mach number. For Mars 2020, more work was done to refine the opening load indicator due to questions about parachute structure during the inflation process. One of the new indicators was suggested by Way [27], who showed the dynamic pressure at full inflation could quantify the momentum captured by the parachute during inflation. This indicator is used by the Mars 2020 mission.

For ASPIRE, a variety of these indicators were used to target the desired flight conditions. Table 3 shows the actual flight conditions achieved and the 50th percentile predictions from pre-flight Monte Carlo simulations. The flight data is generally higher than the predicted values, especially dynamic pressure and Mach number at full inflation. Reconciliation results from Ref. [31] have shown that once the simulation is adjusted for actual simulation initial

Table 2 Targeted flight conditions for the three ASPIRE flights.

Flight	Dynamic Pressure (Pa) at Full Inflation	Parachute Load (lbf) at Full Inflation
SR01	474	35,000
SR02	678	47,000
SR03	950	70,000

conditions and reconstructed atmosphere, the simulation can be reconciled with the flight data.

Table 3 Parachute load comparison across the three ASPIRE flights.

	SR01		SR02		SR03	
Parameter	1st peak	2nd peak	1st peak	2nd peak	1st peak	2nd peak
Flight Chute Load (lbf)	32,387	32,336	50,521	55,982	67,336	66,515
50th Percentile Mars 2020 Indicator (lbf)	35,743	–	47,034	–	66,353	–
50th Percentile C_x=1.15 Max Load (lbf)	–	–	48,606	–	69,941	–
50th Percentile C_x=1.4 Max Load (lbf)	42,005	–	–	–	85,571	–
Flight Dynamic Pressure (Pa)	494.73	466.32	746.50	694.69	1020.12	909.60
50th Percentile Predicted Dynamic Pressure (Pa) at Full Inflation	473.7	–	678.13	–	953.14	–
Flight Mach	1.77	1.71	1.97	1.89	1.85	1.73
50th Percentile Predicted Mach at Full Inflation	1.72	–	1.76	–	1.73	–

Up until SR02, the targets for the flights were based on achieving a certain value at full inflation, where the highest parachute load us typically observed, as seen in Fig. 10(a). The Mars 2020 indicator developed by Way [27] with a proportionality constant tuned for ASPIRE was used for SR01 and SR02 as a surrogate of the target parachute load.

However, one of the discoveries after SR02 was that the second peak of the parachute load was higher than the first peak. A supersonic parachute typically achieves a first peak after the inflation process, then quickly deflates and reinflates, leading to a second peak. Although the first peak at full inflation is typically the largest, SR02 showed a larger peak after the parachute reinflated (see Fig. 10(b)). Both peak loads were accounted for during the targeting process for SR03.

The Mars 2020 indicator is only valid for the full inflation peak. Due to this, for SR03, the process of accounting for the second peak in targeting was solved by tracking the opening load indicator through both peaks. The opening load factor (C_x) was chosen to be 1.15 based on ASPIRE SR01 flight data. The target dynamic pressure at full inflation was selected to be the value where the maximum opening load indicator distribution at either peak had a 50th percentile equal to the targeted load of 70,000 lbf.

B. Parachute Line Loads

Part of the multi-body model involves modeling tension-only bridle lines that connect the payload to the triple bridle confluence point. The model of the bridle lines is numerically stiff and can be sensitive to small changes in line stiffness and damping. However, modeling the line dynamics is crucial; the torque imparted by the motion of the parachute changes the attitude of the payload. While the ASPIRE payload was only instrumentation, but same model was used for MSL and is being used to design the Mars 2020 vehicle, where limiting the attitude dynamics of the payload is important. Hence, post-flight, it is critical to note how well the line loads were recreated by the flight simulation.

Figure 11 shows line load measured for all three ASPIRE flights and compares them with line load predicted from

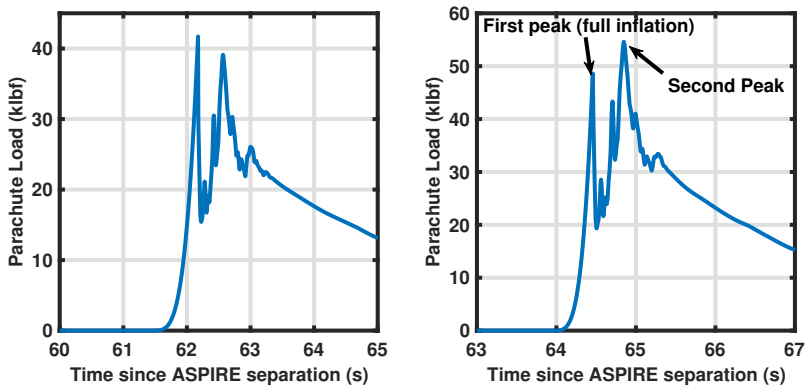

(a) SR01 (b) SR02

Fig. 10 Pre-flight parachute load prediction for SR01 and SR02 with first and second peak noted.

the flight simulation model. The simulation has been adjusted to include the post-flight reconstructed atmosphere and actual states at launch vehicle separation, but otherwise the parachute model is the same as what was used pre-flight. The reconciled flight simulation line load prediction matches the flight inflation curve shapes very well, although there is a discrepancy in the inflation time. The simulation also shows other dynamics post-second peak that are not seen in the flight data. It should be recalled that the flight simulation model of the parachute has no aerodynamic damping, while the real parachute dynamics most likely have some aerodynamic damping.

C. Attitude Dynamics

The metrics that have been presented so far have defined the gross motion of the vehicle, especially predicting the force history; however, the multi-body model is especially important for ASPIRE and for Mars missions like Mars 2020 since it can be used to predict the attitude dynamics of system, especially the attitude history of the payload which is the critical component.

One metric of interest is the parachute pull angle as defined in [25] as the angle between the parachute force vector and the negative axis of symmetry of the payload. This angle is important to the attitude dynamics of the payload and affects the structural loading on the payload if it grows too large. Figure 12 shows the flight reconstruction of the pull angle for SR02 and the flight simulation equivalent. Once again, the flight simulation result has been adjusted to include the post-flight reconstructed atmosphere and actual state at vehicle separation, but the parachute model remains unaltered from its pre-flight form. While the prediction from the simulation is out-of-phase with the flight data, the

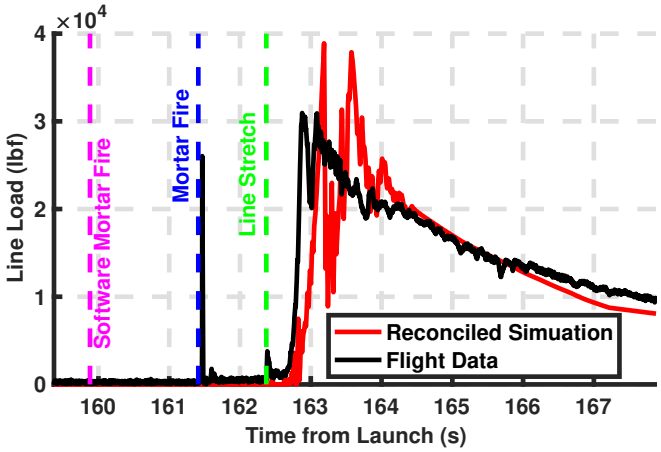

(a) SR01

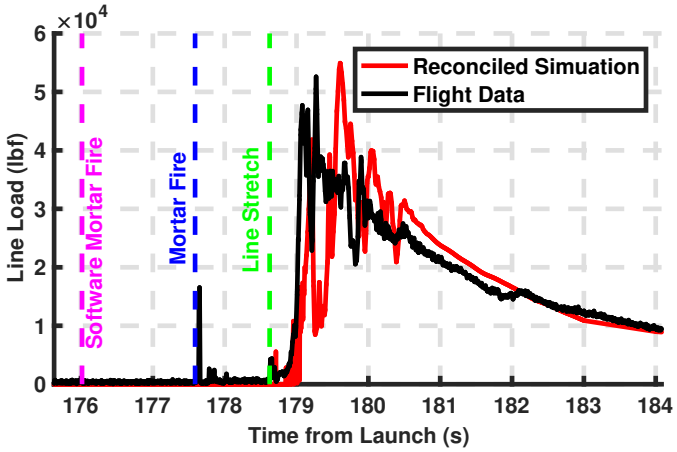

(b) SR02

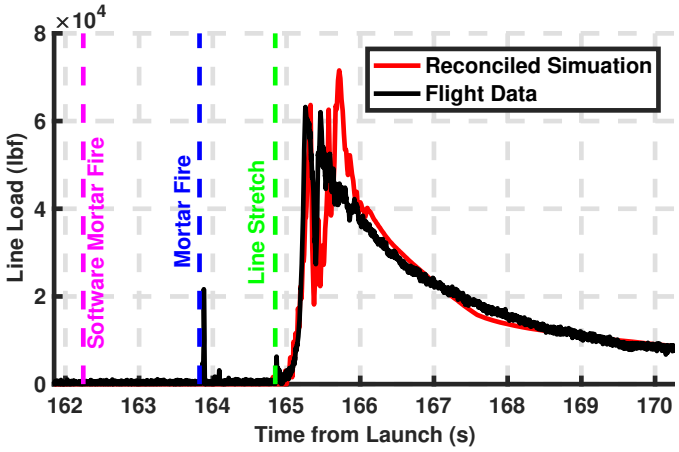

(c) SR03

Fig. 11 Comparison of line load measurement and simulation prediction.

amplitude of the flight data is captured by the simulation. The phasing offset could be a result of small differences in timing between the simulation and the flight data, and is usually less consequential to vehicle performance than the amplitude, which affects structural loads. This result is representative of the comparison of pull angles from SR01 and SR03 data.

Figure 13 shows the Monte Carlo simulation prediction of the maximum pull angle after Mortar Fire in bins of 1-s. The flight data has also been similarly discretized and the maximum binned pull angle for all three ASPIRE flights are shown. One can see that pull angle from the flight data is at at a lower percentile for SR01, while for SR02 and SR03 the pull angle remained close to the median (50th percentile). This means that for SR01, the simulation overpredicted the pull angle between the payload and the parachute and for SR02 and SR03 the predictions were in line with the flight data.

The pull angle predictions are very sensitive to the initial apparate angle of the parachute that is an input to the multi-body simulation as described in Sec. IV. Due to the novelty of ASPIRE having a slender body as a payload for a supersonic parachute, the apparate angle distribution was based on a mix of engineering judgment and extrapolation from blunt-body payload tests. The apparate angle distribution was not modified for any of the ASPIRE flights and the resulting pull angle history from flight seems to have matched pre-flight predictions closely, especially for the latter two flights which used the Mars 2020 parachute article. Due to the observations of the pull angle comparisons for SR02 and SR03, no modifications to the apparate angle were suggested for future flights.

Pull angle can be envisioned as the forcing function of the spring-mass-damper system that is modeled by the bridle lines that connect the parachute vehicle with the payload in the multi-body dynamics model. The resulting output of this system is the attitude rate history of the payload. Figure 14 shows the maximum attitude rate of the payload in 1-s bins

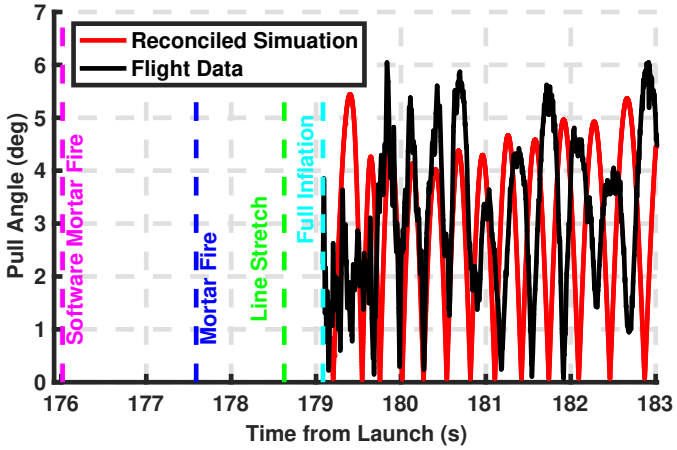

Fig. 12 Comparison of line load derived pull angle and simulation prediction for SR02.

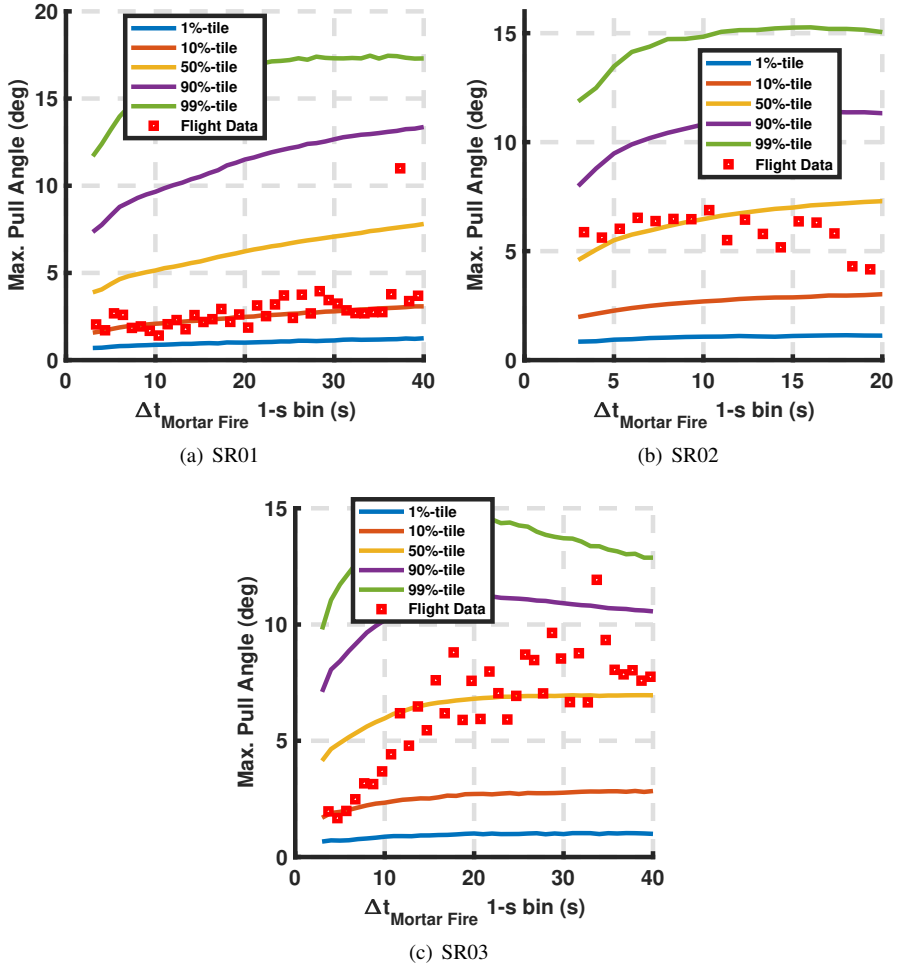

(a) SR01

(b) SR02

(c) SR03

Fig. 13 Comparison of pull angle between flight data and Monte Carlo simulation predictions.

from the Monte Carlo and the flight data. The simulation overpredicts attitude rate compared to the flight data for SR01 and SR03, while for the first 20 s after mortar fire in ASPIRE SR02 the reconstructed attitude rate is approximately near

the 50th percentile of the simulation prediction.

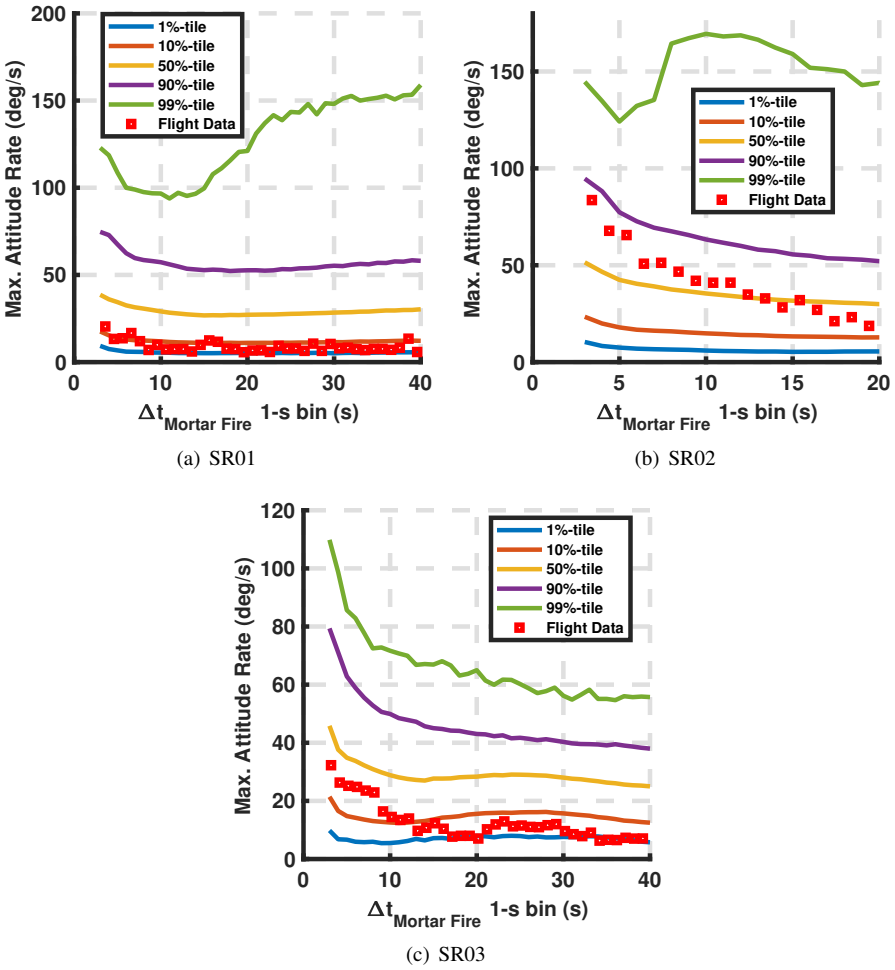

(a) SR01

(b) SR02

(c) SR03

Fig. 14 Comparison of maximum attitude rate of the payload between flight data and Monte Carlo simulation predictions.

The inputs for the multi-body dynamics models were selected conservatively prior to the ASPIRE flights to produce bounding predictions from the simulation. Thus, it is not surprising that the resulting attitude rates from the simulation are overpredictions. Apparate angle distribution can be modified to empirically move the 50th percentile of the simulation prediction to match the flight data, as has been done for the Mars 2020 simulation based on MSL flight data. For ASPIRE, such tuning was not considered since the simulation predictions were still bounding, allowing for margin in the system. The ASPIRE experience for the apparate angle distribution does not translate over to Mars 2020, since that mission has a blunt-body for a payload. However, if a future parachute testing program with a slender-body uses this muti-body model in the future for predictions, the apparate angle distribution could be tuned based on the ASPIRE dataset.

D. Inflation Time

As described in Sec. IV, the ASPIRE simulation used the inflation length method as described by Greene [26] to compute the time it takes for the parachute to inflate. The method uses a proportionality factor called the inflation alpha to characterize the distance the parachute needs to travel before it is fully inflated. Reference [3] looked at historic data of Earth-based supersonic parachute tests and successful flights at Mars to determine a distribution of inflation alpha for the ASPIRE flights. For SR01, this distribution was a uniform distribution between 4 and 10. However, looking at the pre-flight prediction of inflation time and comparing it to actual flight data in Fig. 15(a), the flight data was a low

probability event. The inflation time predicted by the simulation was a wide range, especially when also compared to recent inflation times observed for other Earth-based tests such as the LDSD flights.

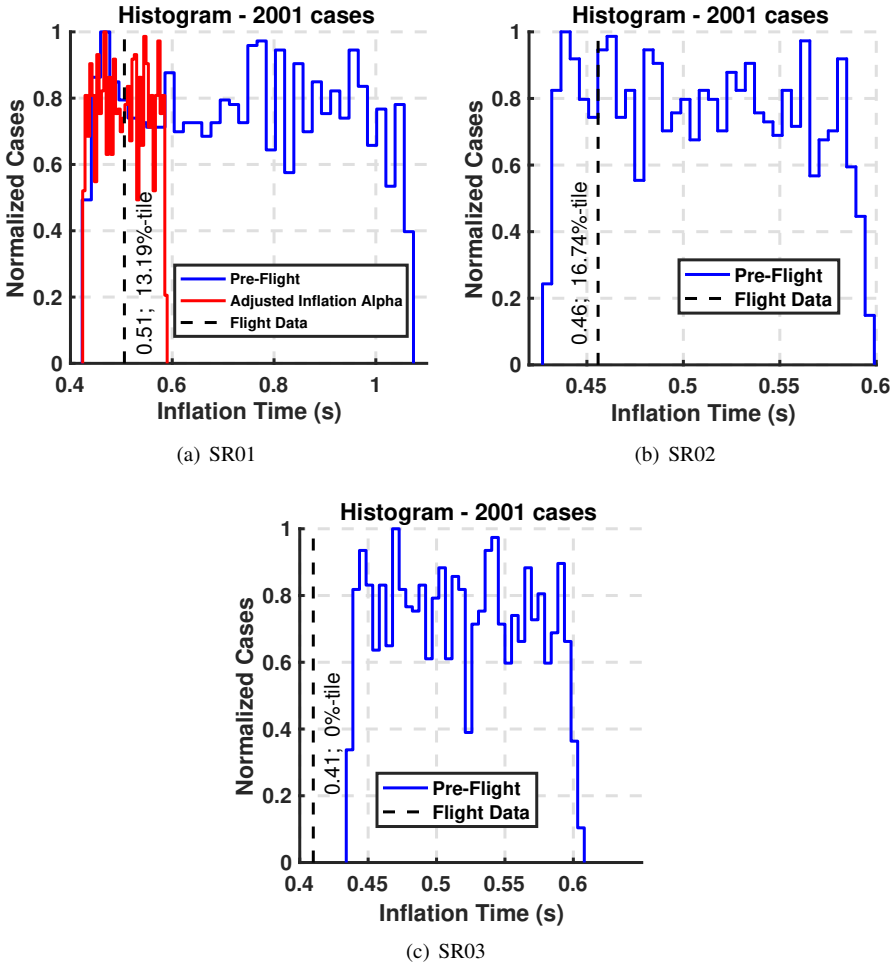

(a) SR01

(b) SR02

(c) SR03

Fig. 15 Comparison of inflation time between flight data and Monte Carlo simulation prediction.

For SR02, the inflation alpha distribution was narrowed based on the SR01 experience to a uniform distribution of 4 to 5.5. This distribution was tested with the SR01 simulation and the actual inflation time appeared to be the median of the predicted inflation time as seen in Fig. 15(a). However, when SR02 inflation time was compared with the pre-flight estimate of inflation time for that flight, shown in Fig. 15(b), the inflation time for was once again faster than the predicted time. There was a hypothesis that inflation time might be correlated with the dynamic pressure during the inflation process, but due to a small sample of data, the inflation alpha distribution remained unchanged between SR02 and SR03.

When SR03 data was compared its pre-flight estimate, the flight data was outside the bounds of the pre-flight prediction as seen in Fig. 15(c). Once again, actual inflation time was faster than what was predicted. The SR03 flight was another sample in supporting the hypothesis that higher dynamic pressure leads to faster inflation when all things are kept constant. Since there was no follow-on to ASPIRE SR03, the inflation alpha distribution was not modified after the flight. If there is a similar flight that targets a higher dynamic pressure, the inflation alpha model should be modified to bound the inflation time within the simulation. However, Mars 2020, the program that used ASPIRE as a risk mitigation exercise is targeting a much lower dynamic pressure - approximately 500 Pa - the inflation alpha distribution for that program remains unchanged.

E. Splashdown Time

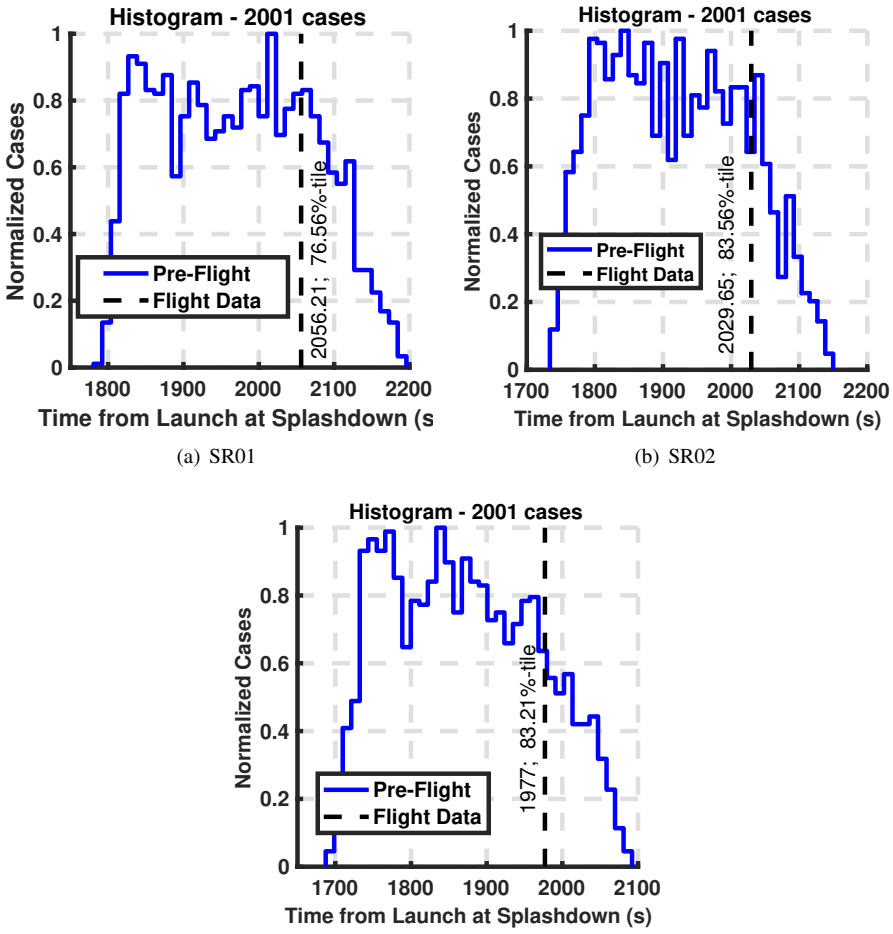

(a) SR01

(b) SR02

(c) SR03

Fig. 16 Comparison of splashdown time between flight data and Monte Carlo simulation prediction.

The ASPIRE multi-body simulation was also used to produce splashdown time predictions, which was useful for recovery operations. Using the static aerodynamics tables described in Sec. III.B, the ASPIRE parachute can trim at two very different angles - approximately 6 deg and 14 deg total angle of attack - which in turn produce very different lift-to-drag ratios and time on parachutes. From, Fig. 16, one can see that the time on parachute statistics from a Monte Carlo analysis with the multi-body simulation enveloped the actual splashdown times from all three flights, albeit the predictions in general underpredicted the splashdown time; however, what is not shown in these plots is that the splashdown time estimate from a drag-only modeling of the parachute produced a lot lower estimate of the splashdown time, which would not envelop the actual splashdown times. It was also observed that Monte Carlo cases with the higher trim point (approximately 14 deg) were correlated with the longer splashown times similar to what was observed in the actual flight.

One can theorize that if model changes were made to adjust the frequency of the higher trim point in the simulation, by adjusting the bounds of pitching moment and normal force coefficients in the static aerodynamics, the splashdown time predictions in Fig. 16 could be shifted to the right, making the flight data more centered in the statistics. However, parachute reconstruction by O'Farrell [28], Muppidi [24], and Sonneveldt [32] show that the drag performance of the vehicle was very close to what was the nominal value seen in Figs. 6 and 8 and there was no appreciable bias in the observed drag as one would expect with a higher than nominal trim point, especially in the subsonic portion of flight where the parachute spends most of its time during its descent to the ground. Thus, no model changes were suggested due to lack of reconstruction data that proved that models should be adjusted to increase the frequency of the higher

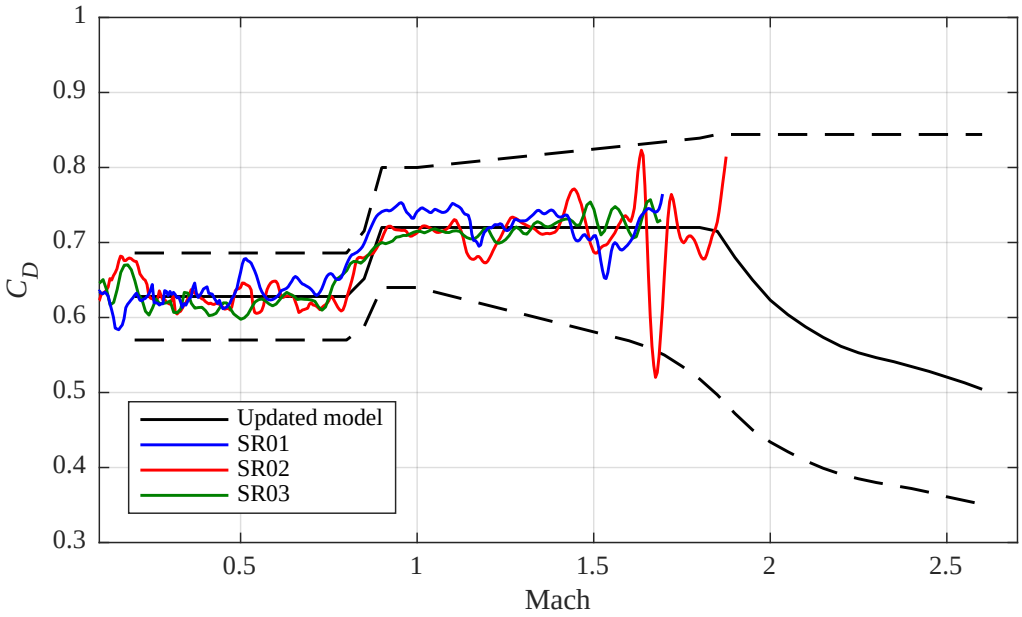

Fig. 17 Updated drag coefficient model proposed by [24] post ASPIRE flights.

trim point. There might be other explanations for the underprediction of the splashdown time by simulation, including the presence of higher than expected vertical winds. Unfortunately, ASPIRE did not have an on-board anemometer to corroborate this hypothesis.

F. Modeling Changes

Based on good comparison between the flight data and the simulation predictions for line load metrics for the three flights, no changes were made to the modeling of the lines and multi-body dynamics. Between SR01 and SR02, the line properties were modified in the simulation as the project shifted the test article from the MSL built-to-print article to the Mars 2020 strengthened parachute. However, as seen in Table 3 and in Fig. 11, the actual parachute load and line loads from the flight remained in family with the predictions from the simulation. The inputs for attitude dynamics, such as the apparate angle distribution, were similarly not adjusted as the flight data was in family with the predictions from the simulation, and there was positive margin between simulation predictions that were factored in vehicle design and the actual flight data. There were modeling changes made for the inflation time calculation between SR01 and SR02 based on flight data, but as Fig. 15(c) showed, ASPIRE SR03 inflation time was not enveloped by the inflation time predicted by the simulation. There might be other physics not captured in the inflation time model, such as a dependency on dynamic pressure, but since Mars 2020, the customer for ASPIRE, has a lower target dynamic pressure, no model changes were pursued at the end of ASPIRE. Finally, the simulation underpredicted the splashdown time for all three flights, but there was no reconstructed aerodynamic data found to suggest a model change, especially since the simulation predictions still enveloped the flight data.

Muppidi et al. [24] presented a modified drag coefficient model for ASPIRE post-flight. The model used for ASPIRE, which was shown in Fig. 6, was updated as the three ASPIRE flights consistently did not exhibit the drag bucket phenomena near Mach 1 nor did the drag coefficient reduce significantly at higher than Mach 1.5. Based on these observations, the post-flight model (Fig. 17) had tighter bounds in the subsonic region, the drag bucket feature was replaced by a linear ramp from subsonic to supersonic drag, and the supersonic drag coefficient was fixed to a drag coefficient on the upper bound.

[24] did not suggest any changes for the static aerodynamics model – tangential, normal, and pitching moment coefficient. The static aerodynamics are more instrumental in the implementation of the multi-body dynamics. The observed flight data from ASPIRE did not provide enough data to reconstruct these aerodynamic quantities. Hence, the changes suggested by [24] are not expected to change performance predictions from the multi-body simulation.

VI. Conclusions

The ASPIRE project served as a parachute qualification and risk mitigation exercise by the Mars 2020 project using a series of sounding rocket tests. In October 2017, ASPIRE SR01 tested the MSL-heritage DGB parachute and deployed the decelerator near conditions seen by the MSL mission on Mars in 2012. In March 2018, ASPIRE SR02 successfully tested a new strengthened DGB parachute at a dynamic pressure that was fifty percent higher than what was seen by MSL. In September 2018, ASPIRE SR03 tested the new DGB parachute at twice the load expected by the Mars 2020 flight. A multi-body flight dynamics simulation was developed to provide pre-flight vehicle performance predictions and was used to target Mars relevant parachute deployment conditions. The simulation incorporated various engineering models, specifically the 6DOF parachute aerodynamics. The three ASPIRE flights showed that the multi-body dynamics model performed favorably when compared to the flight data and did not need any major adjustments to meet the needs of the ASPIRE or Mars 2020 projects.

Acknowledgments

Clara O'Farrell contributed significantly to this paper, especially with information for the parachute aerodynamic modeling. The author would like to acknowledge several ASPIRE team members who have contributed to the flight mechanics work presented in this papers. These team members include Eric Queen, Angela Bowes, Mark Ivanov, Emily Leylek, Chris Karlgaard, Jake Tynis, Brian Sonneveldt, John Van Norman, Suman Muppidi, Ian Clark, Juan Cruz, William Strauss, Nic Marks, and David Way. Parts of this research were carried out at the Jet Propulsion Laboratory, California Institute of Technology, under a contract with the National Aeronautics and Space Administration.

References

[1] Tanner, C., Clark, I., , and Chen, A., "Overview of the Mars 2020 Parachute Risk Reduction Plan," *IEEE Aerospace Conference 2018,* Big Sky, MT, 2018.

[2] Cruz, J. R., Way, D. W., Shidner, J. D., Davis, J., Adams, D. S., and Kipp, D., "Reconstruction of the Mars Science Laboratory Parachute Performance," *Journal of Spacecraft and Rockets*, Vol. 51, No. 4, 2014, pp. 1185–1196.

[3] O'Farrell, C., Muppidi, S., Brock, J., Van Norman, J., and Clark, I., "Development of Models for Disk-Gap-Band Parachutes Deployed Supersonically in the Wake of a Slender Body," *IEEE Aerospace Conference,* Big Sky, MT, 2017.

[4] Reichneau, D. E. A., "Aerodynamic Characteristics of Disk-Gap-Band Parachutes in the Wake of Viking Entry Forebodies at Mach Numbers From 0.2 to 2.6," Tech. rep., AEDC-TR-72-78, 1972.

[5] Cruz, J. R., O'Farrell, C., Zumwalt, C. H., and Keller, D. F., "Wind Tunnel Testing of Ringsail and Disk-Gap-Band Parachutes," Tech. rep., NESC TAR 14-00932, 2015.

[6] Sengupta, A., Roeder, J., Kelsch, R., Wernet, M., Kandis, M., and Witkowski, A., "Supersonic Disk Gap Band Parachute Performance in the Wake of a Viking-Type Entry Vehicle from Mach 2 to 2.5," AIAA Paper No. 2008-6217*, AIAA Atmospheric Flight Mechanics Conference 2016,* Honolulu, HI, 2008.

[7] Muppidi, S., O'Farrell, C., Tanner, C., Van Norman, J., and Clark, I., "Modeling and Flight Performance of Supersonic Disk-Gap-Band Parachutes In Slender Body Wakes," AIAA Paper No. 2018-3623 *AIAA Aviation Conference 2018,* Atlanta, GA, 2018.

[8] Zumwalt, C., Cruz, J., O'Farrel, C., and Keller, D., "Wind Tunnel Test of Subscale Ringsail and Disk-Gap-Band Parachutes," AIAA Paper No. 2016-3882*, AIAA Aviation Conference 2016,* Washington, DC, 2016.

[9] Cruz, J. R., Mineck, R. E., Keller, D. F., and Bobskill, M. V., "Wind Tunnel Testing of Various Disk-Gap-Band Parachutes," AIAA Paper No. 2003-2129*, AIAA Aerodynamic Decelerator System 2003,* Monterey, CA, 2003.

[10] Cruz, J. R., and Snyder, M. L., "Estimates for the Aerodynamic Coefficients of Ringsail and Disk-Gap-Band Parachutes Operating on Mars," AIAA Paper No. 2017-4055*, AIAA Aviation 2017,* Denver, CO, 2017.

[11] Cruz, J. R., O'Farrell, C., Hennings, E., and Runnels, P., "Permeability of Two Parachute Fabrics - Measurements, Modeling, and Application," Tech. rep., TM 2016-219328, 2016.

[12] Braun, R. D., Powell, R. W., Engelund, W. C., Gnoffo, P. A., Weilmuenster, K. J., and Mitcheltree, R. A., "Mars Pathfinder Six-Degree-of-Freedom Entry Analysis," *Journal of Spacecraft and Rockets*, Vol. 32, No. 6, 1995, pp. 993–1000. doi: 10.2514/3.26720.

[13] Desai, P. N., Schoenenberger, M., and Cheatwood, F. M., "Mars Exploration Rover Six-Degree-of-Freedom Entry Trajectory Analysis," *Journal of Spacecraft and Rockets*, Vol. 43, No. 5, 2006, pp. 1019–1025. doi:10.2514/1.6008, URL `http://doi.aiaa.org/10.2514/1.6008`.

[14] Desai, P. N., Prince, J. L., Queen, E. M., Schoenenberger, M., Cruz, J. R., and Grover, M. R., "Entry, Descent, and Landing Performance of the Mars Phoenix Lander," *Journal of Spacecraft and Rockets*, Vol. 48, No. 5, 2011, pp. 798–808. doi:10.2514/1.48239.

[15] Way, D. W., Davis, D., Jody, and Shidner, J. D., "Assessment of the Mars Science Laboratory Entry, Descent, and Landing Simulation," AAS 13-420*, AAS/AIAA Space Flight Mechanics Conference,* Kauai, HI, 2013.

[16] Bowes, A., Davis, J. D., Dutta, S., Striepe, S., Ivanov, M., Powell, R., and White, J. P., "LDSD POST2 Simulation and SFDT-1 Pre-flight Launch Operations Analyses," AAS 15-232, *AAS/AIAA Space Flight Mechanics Conference,* Williamburg, VA, 2015.

[17] White, J., Dutta, S., and Striepe, S., "SFDT-1 Camera Pointing and Sun-Exposure POST2 Analysis and Flight Performance," AAS 15-218, *AAS/AIAA Space Flight Mechanics Conference,* Williamburg, VA, 2015.

[18] Dutta, S., Bowes, A., Striepe, S., Davis, J. D., Blood, E. M., and Ivanov, M., "Supersonic Flight Dynamics Test 1 - Post-flight Assessment of Simulation Performance," AAS 15-219, *AAS/AIAA Space Flight Mechanics Conference,* Williamsburg, VA, 2015.

[19] White, J. P., Bowes, A., Dutta, S., Ivanov, M., and Queen, E., "LDSD POST2 Modeling Enhancements in Support of SFDT-2 Flight Operations," AAS 16-221, *AAS/AIAA Space Flight Mechanics Conference,* Napa, CA, 2016.

[20] Dutta, S., Bowes, A., White, J., Striepe, S., Queen, E., O'Farrell, C., and Ivanov, M., "Post-Flight Assessment of Low Density Supersonic Decelator Flight Dynamics Test 2 Simulation," AAS 16-222, *AAS/AIAA Space Flight Mechanics Conference,* Napa, CA, 2016.

[21] Leslie, F., and Justus, C., "The NASA Marshall Space Flight Center Earth Global Reference Atmosphere Model - 2010 Version," Tech. rep., NASA/TM-2011-216467, 2011.

[22] Molod, A., Takacs, L., Suarez, M., Bacmeister, J., Song, I., and Eichmann, A., "The GEOS-5 Atmospheric General Circulation Model: Mean Climate and Development from MERRA to Fortuna," Tech. Rep. NASA TM 2012-104606-VOL-28, NASA GFSC, 2012.

[23] Toniolo, M., Tartabini, P., Pamadi, B., and Hotchko, N., "Constraint Force Equation Methodology for Modeling Multi-Body Stage Separation Dynamics," AIAA 2008-219, *AIAA Aerospace Sciences Meeting and Exhibit,* Reno, NV, 2008.

[24] Muppidi, S., O'Farrell, C., Van Norman, J., and Clark, I., "ASPIRE Aerodynamic Models and Flight Performance," AIAA Paper No. 2019-3376 *AIAA Aviation Conference 2019,* Dallas, TX, 2019.

[25] Cruz, J., Way, D., Shidner, J., Davis, J., Powell, R., Kipp, D., Adams, D., Sengupta, A., Witkowski, A., and Kandis, M., "Parachute Models Used in the Mars Science Laboratory Entry, Descent, and Landing Simulation," AIAA 2013-1276, *AIAA Aerodynamic Decelerator Systems (ADS) Conference,* Daytona Beach, FL, 2013.

[26] Greene, G., "Opening Distance of a Parachute," *Journal of Spacecraft*, Vol. 7, No. 1, 1970, pp. 98–100. doi:10.2514/3.29878.

[27] Way, D., "A Momentum-Based Indicator for Predicting the Peak Opening Load of Supersonic Parachutes," IEEE Paper No. *IEEE Aerospace Conference,* Big Sky, MT, 2018.

[28] O'Farrell, C., Karlgaard, C., Tynis, J., and Clark, I., "Overview and Reconstruction of the ASPIRE Project's SR01 Supersonic Parachute Test," *IEEE Aerospace Conference,* Big Sky, MT, 2018.

[29] Karlgaard, C., Tynis, J., and O'Farrell, C., "Reconstruction of the Advanced Supersonic Parachute Inflation Research Experiment (ASPIRE) Sounding Rocket Flight Test," AIAA Paper No. 2018-3624 *AIAA Atmospheric Flight Mechanics Conference,* Atlanta, GA, 2018.

[30] Karlgaard, C., Tynis, J., O'Farrell, C., and Sonneveldt, B., "Reconstruction of the Advanced Supersonic Parachute Inflation Research Experiment Sounding Rocket Flight Tests with Strengthened Disk-Gap-Band Parachute," AIAA Paper No. 2019-0014 *AIAA Science and Technology Conference,* San Diego, CA, 2019.

[31] Dutta, S., Queen, E., Bowes, A., Leyleck, E., and Ivanov, M., "ASPIRE Flight Mechanics Modeling and Post Flight Analysis," AIAA 2018-3625*, AIAA Aviation 2018, AIAA Atmospheric Flight Mechanics Conference,* Atlanta, GA, 2018.

[32] Sonneveldt, B., O'Farrell, C., and Clark, I., "Summary of the Advanced Supersonic Parachute Inflation Research Experiments (ASPIRE) Sounding Rocket Tests with a Disk-Gap-Band Parachute," AIAA 2019-3482*, AIAA Aviation 2019,* Dallas, TX, 2019.